Photoemission of the SiO_2–SiC heterointerface

M. L. O'Brien, C. Koitzsch and R. J. Nemanich

Citation: Journal of Vacuum Science & Technology B: Microelectronics and Nanometer Structures Processing, Measurement, and Phenomena **18**, 1776 (2000); doi: 10.1116/1.591471

View online: https://doi.org/10.1116/1.591471

View Table of Contents: https://avs.scitation.org/toc/jvn/18/3

Published by the American Institute of Physics

ARTICLES YOU MAY BE INTERESTED IN

Band offsets of wide-band-gap oxides and implications for future electronic devices
Journal of Vacuum Science & Technology B: Microelectronics and Nanometer Structures Processing, Measurement, and Phenomena **18**, 1785 (2000); https://doi.org/10.1116/1.591472

Bandtails and defects in microcrystalline silicon (μc-Si:H)
Journal of Vacuum Science & Technology B: Microelectronics and Nanometer Structures Processing, Measurement, and Phenomena **18**, 1792 (2000); https://doi.org/10.1116/1.591473

Band offsets and electronic structure of SiC/SiO_2 interfaces
Journal of Applied Physics **79**, 3108 (1996); https://doi.org/10.1063/1.361254

Silicon oxycarbide formation on SiC surfaces and at the SiC/SiO_2 interface
Journal of Vacuum Science & Technology A **15**, 1597 (1997); https://doi.org/10.1116/1.580951

The valence band alignment at ultrathin SiO_2/Si interfaces
Journal of Applied Physics **81**, 1606 (1997); https://doi.org/10.1063/1.363895

Investigation of nitric oxide and Ar annealed SiO_2/SiC interfaces by x-ray photoelectron spectroscopy
Journal of Applied Physics **86**, 4316 (1999); https://doi.org/10.1063/1.371363

Photoemission of the SiO_2–SiC heterointerface

M. L. O'Brien, C. Koitzsch, and R. J. Nemanich[a)]
Department of Physics, North Carolina State University, Raleigh, North Carolina 27695-8202

(Received 25 February 2000; accepted 28 February 2000)

Photoelectron spectroscopy has been performed on SiC surfaces to investigate the valence band characteristics during SiO_2 formation. Various stages of the oxide development were investigated. The $\sqrt{3}\times\sqrt{3}R30°$ surface is used as the initial surface for the oxidation experiments. The substrates were exposed to a succession of a 30 s oxygen exposure, two 30 s oxygen plasmas, and finally, a plasma-enhanced chemical vapor deposition SiO_2 deposition. Ultraviolet photoemission spectroscopy was employed to measure the valence band discontinuity for the oxide on *n*-type 6H and *n*-type 4H SiC substrates for each step in the oxidation process. X-ray photoemission spectroscopy was used to confirm the valence band offset. The valence band discontinuity was determined to be 2.0 eV. Furthermore, the location of the valence band maximum of the SiC to the conduction band minimum of the SiO_2 is determined to be a constant (~7.0 eV) between 6H and 4H SiC. Band bending effects are directly measured from ultraviolet photoemission spectroscopy (UPS) and x-ray photoemission spectroscopy. From the UPS measurements of the band bending effects, the interface state density is determined to be $\sim 5\times10^{12}\,\mathrm{cm}^{-2}$. © *2000 American Vacuum Society.* [S0734-211X(00)11003-0]

I. INTRODUCTION

The electronic structure of SiC heterojunctions is of interest because of the high potential this material possesses for electronic applications. Silicon carbide devices promise outstanding performance parameters due to the physical and electronic properties of the material, such as wide band gap, high thermal conductivity, and high electron mobility. The wide band gap (3.02, 3.26, and 2.4 eV for 6H, 4H, and 3C, respectively), excellent thermal conductivity, and high saturated electron drift velocity are important for high power, high frequency, and high temperature operations.[1–6] SiC has long been considered as an ideal material for high power devices, and is favored over other wide-band-gap materials. Much of the interest arises because of its ability to be thermally oxidized to form SiO_2. The thermal oxidation properties of SiC make it ideal for metal–oxide-semiconductor (MOS) structures, and MOS gated devices are important for certain high power applications.[7] The MOS structure entails a layered structure of metal–oxide–semiconductor. The thermal oxidation of SiC enables passivation and local oxidation to allow for integrated circuits on a single chip. Furthermore, the electrical properties of SiO_2 for integrated circuit and device fabrication have been thoroughly investigated in silicon technology. However, the thermal oxidation of silicon carbide has proven to be more complicated than that of silicon. Therefore, an understanding of the SiC SiO_2 interface is important for the development of SiC as a viable material for MOS structure fabrication. Band bending behavior, band discontinuities, and interface state distributions are key considerations for device design. Interface state densities below $10^{11}\,\mathrm{cm}^{-2}$ are needed to ensure reliable device operation.

A significant issue for thermal oxidation of SiC is the removal of the carbonaceous species from the interface and the oxidized film. The transport of the species to the gas phase generates CO and CO_2 molecules which must diffuse to the surface. Studies have shown that the oxidation of silicon in a slight CO and CO_2 atmosphere results in an increase in surface roughness and bubble formation throughout the grown oxide. It results in a significant degradation in electronic properties, such as increased interface state density, decreased generation lifetime, and increased surface recombination velocity.[8] The same effects may be expected for the oxidation of SiC. The oxidation of silicon carbide has been shown to generate a higher interface state density than for the oxidation of silicon, which may be a result of carbonaceous species diffusing through the oxide. It has been suggested that the interface states are related to sp^2-bonded carbon clusters.[9,10] The reduction of the interface state density of silicon carbide is of great importance to the utilization of SiC as an MOS device material.

Examining and monitoring the band bending and band offsets during the initial oxidation of silicon carbide will present information about the SiC/SiO_2 interface. Prior studies have shown a lower interface state density for the oxidation of the Si face of SiC as opposed to the C face.[8] The reaction of oxygen with the Si face of SiC has been shown to be slower than the carbon face. It has been suggested that the slower oxidation rate allows for a lower concentration of by-products diffused through the oxide.[11,12] Therefore, this study will focus on the Si face of SiC.

Thermal oxidation of silicon carbide has been extensively examined. It has been shown that there is a strong influence of the oxidation conditions on the quality of the oxide for cubic (β) SiC. It has been determined that the interface state density is an order of magnitude lower for wet oxidation than dry.[13,14] Further investigation has shown that by using an off-axis substrate, the interface state density and fixed charge characteristics improve. In addition, the interface density can

[a)]Electronic mail: Robert_Nemanich@ncsu.edu

be reduced to $\sim 10^{10}\,cm^{-2}\,eV^{-1}$, by using various oxidation and reoxidation steps in the thermal oxidation process. Using these processes, the interface state density of the SiO_2/SiC interface approaches that of the Si–SiO_2 interface.[13–15]

Oxides on hexagonal (α) polytypes of silicon carbide have also been studied. It was found that the primary cause for SiC MOS field-effect transistor (FET) device failure is leakage and breakdown of the gate insulator.[16] A more focused study of the application of oxides on α-SiC addressed issues related to obtaining a functioning high-power device. It was found that oxidation of the hexagonal as well as cubic polytypes resembled the Deal–Grove model developed to explain the thermal oxidation of silicon.[17] The Deal–Grove model describes the oxidation of silicon as two process: (1) surface reaction limited, and (2) limited by diffusion for SiO_2 formation.[18,19]

Thermal oxidation of *p*-type SiC has further complications. The thermal oxide that is grown on a *p*-type substrate exhibits a significantly higher interface state density than on *n*-type substrates.[16] Several models have been proposed to account for this. One model suggests a redistribution of the Al dopant into the oxide generates defects. However, similar results were found using boron as *p*-type dopants.[20–22] Boron has a high solubility in SiO_2 and does not generate significant defect densities for oxidation of silicon. The thermal oxidation of *p*-type SiC continues to present problems to the development of SiC technologies.

In order to solve the problem of oxidation for α-SiC, novel methods are being proposed. Since it has been shown that a reoxidation step improves the quality of the oxide,[22] plasma treatments are being investigated for both pre- and post-oxidation treatments to improve the oxide quality. It has been shown that plasma treatments before oxidation can improve oxide quality by reducing the interface state densities.[23–25] Furthermore, nitridation of the SiO_2/SiC interface has also been shown to reduce the interface state densities.[26–28] Another proposed solution for the fabrication of MOS structures on *p*-type α-SiC is to use deposited oxides as the gate dielectrics. In fact, recent results have shown that deposited oxides may prove to be acceptable for forming gate oxides on SiC.[23,27,29]

Investigation by internal photoemission into several polytypes (3C, 6H, 4H, and 15R) shows that the energy difference between the SiC valence band edge to the oxide conduction band is a constant (6 eV). Therefore, the SiC band gap determines the location of the conduction band of the SiC relative to the oxide bands.[42] The SiO_2 band gap of $\sim$9 eV indicates that the valence band offset is 3.0 eV for the several SiC polytypes examined. This implies that the SiC band gap is approximately located in the middle of the SiO_2 gap. The indication that the SiC band gap is approximately midgap of the SiO_2 is another advantage of using SiO_2 as an insulator on SiC.

This study focuses on the oxidation of SiC with hexagonal symmetry. The 4H or 6H stacking sequences were used because these polytypes are commercially available and have been used as substrates for electronic device fabrication. A variety of surface reconstructions can be obtained for α-SiC (0001). The reconstructions that have been observed for the Si surface of hexagonal SiC are 1×1, 3×3, $\sqrt{3}\times\sqrt{3}$, and $6\sqrt{3}\times6\sqrt{3}$. In this study, surfaces with a $\sqrt{3}\times\sqrt{3}$ low-energy electron diffraction (LEED) pattern are prepared and studied for the oxidation of SiC. The $\sqrt{3}\times\sqrt{3}$ surface was selected because uniform, nearly stoichiometric surfaces can be prepared. The 3×3 surface is significantly Si rich, and is subject to significant variations in the Si/C ratio. Alternatively, the $6\sqrt{3}\times6\sqrt{3}$ surface is significantly carbon rich. It has been proposed that there are graphitic clusters on the surface.[30] Furthermore, the $\sqrt{3}\times\sqrt{3}$ surface has had notable work preformed to determine its structure and composition. Scanning tunneling microscopy (STM) has displayed the surface structure,[30] while UV photoemission and high-resolution x-ray photoemission have been preformed to examine the electronic and chemical nature of the $\sqrt{3}\times\sqrt{3}$ surface.[31–38]

In this study, ultraviolet photoemission spectra of the valence band are obtained after different stages of the interface formation process. The interface is formed by using a series of oxygen plasma processes. The plasma processes were used because the remote plasma-enhanced chemical vapor deposition (RPECVD) oxides have shown promise in gate oxides on SiC.[23–25] From these spectra, information of the surface electronic structure and electron affinity is obtained. From this insight, the electronic properties of the SiC/SiO_2 heterojunction are obtained.

II. EXPERIMENTAL PROCEDURE

The substrates used were sections of on-axis SiC wafers supplied by Cree Research Inc. The sample size is approximately $1\,cm\times1\,cm$. The wafers were wet chemically cleaned prior to introduction into an integrated ultrahigh vacuum (UHV) system.[39] The wet chemical cleaning consisted of a 5:1:1 H_2O:H_2O_2:NH_4OH bath at 85 °C followed by a DI rinse. Tungsten was then sputtered on the backside to ensure sufficient heat transfer between the radiative heater and the substrate. The substrates were then exposed to a series of cleans consisting of UV/O_3 oxidation followed by a 10:1 HF dip followed by a DI water rinse. The substrates used were *n*-type 6H–SiC ($\rho=0.058\,\Omega$ cm) and 4H–SiC ($\rho=0.039\,\Omega$ cm). The bulk Fermi levels for each substrate were determined by the graphical method outlined by Size.[18] The deduced values for the location of the Fermi level relative to the valence band maximum (VBM) for the 6H and 4H *n*-type substrates are 2.94 and 3.20 eV, respectively.

All measurements were completed in an interconnected system employed for surface processing and characterization. The multichamber system is connected through UHV sample transfer and includes ultraviolet photoemission spectroscopy (UPS), x-ray photoemission spectros-copy (XPS), LEED, Auger electron spectroscopy (AES), remote plasma processing, and Si e-beam deposition. These capabilities were contained in five separate chambers of the system.

The substrates where prepared *in vacu* to obtain a $\sqrt{3}\times\sqrt{3}$ surface reconstruction. The $\sqrt{3}\times\sqrt{3}$ reconstructed surface is obtained first by generating a 3×3 reconstructed sur-

face. The 3×3 surface is produced by annealing the SiC substrate to ~850 °C in a Si flux generated by e-beam evaporation. After the 3×3 surface is obtained, a remote H-plasma treatment is preformed. The remote hydrogen plasma is attained with a 76 sccm flow of H_2 through a quartz tube located ~40 cm above the substrate. The plasma is excited with 20 W of 13.56 MHz rf power. After the H-plasma treatment, the substrate is annealed to 700 °C for 5 min. The resultant LEED reconstruction is $\sqrt{3}\times\sqrt{3}$. The plasma processing of the 3×3 surface ensures no oxygen contamination or graphitization of the surface.

A series of oxygen exposures followed the preparation of the clean $\sqrt{3}\times\sqrt{3}$ surface. The substrates are first exposed to a flow of 20 sccm of O_2 and 100 sccm of He for 30 s at room temperature. The next two exposures to the substrates are remote oxygen plasma for 30 s at 100 °C. The remote oxygen plasma is generated at approximately 40 cm above the substrate by a rf source (13.56 MHz). An oxygen flow of 20 sccm, a helium flow of 100 sccm, and plasma power of 20 W are used to form a thin SiO_2 layer on the surface. Finally, a SiO_2 film is deposited on the surface. The oxide deposition was preformed by RPECVD at 450 °C. In the process, 20 sccm of O_2 and 100 sccm of He are excited by 20 W rf power using the same system. 20 sccm of 1% SiH_4 in He is introduced at the substrate surface through a gas dispersion ring. The RPECVD deposited a thin SiO_2 layer (~15 Å thick) on the surface.

UPS analysis was performed on the clean surface and after each oxygen exposure. The UPS was performed in a Mu metal lined chamber using a VSW HA50 hemispherical analyzer ($r_{\mathrm{mean}}=50\,\mathrm{mm}$) with energy resolution of 0.10 eV and acceptance angle of 2° that is mounted on a dual-axis goniometer. The UV light is generated with a differentially pumped noble gas resonance lamp. Using the He I_α line ($E_0=21.2\,\mathrm{eV}$), the system pressure rose from 4.5×10^{-10} to 5×10^{-9} Torr. However, the increased noble gas partial pressure is not expected to cause sample contamination. For all spectra, a −2.0 V bias was applied to the substrate to ensure that the photoemitted electrons would overcome the work function of the analyzer. All UPS spectra were normalized to the Fermi level of the system. The Fermi level was determined by measuring a clean molybdenum surface in electrical contact with the sample.

XPS was used to examine the Si 2p, C 1s, and O 1s core levels after each oxygen exposure. The sensitivity of the VG Clam II XPS analyzer is such that the core level splitting is not observable. XPS was preformed using an Al anode ($h\nu=1486.6\,\mathrm{eV}$) at 20 mA and 12 kV. The Si 2p core level is measured to provide information about the Si–O bonding. Investigation of the O 1s core level was used as an indication of the oxygen concentration on the surface. Furthermore, the C 1s core level is examined to determine C–O bonding concentration.

III. RESULTS

In this study, UPS and XPS are used to describe the initial oxidation and growth of SiO_2 on the $\sqrt{3}\times\sqrt{3}$ SiO surfaces.

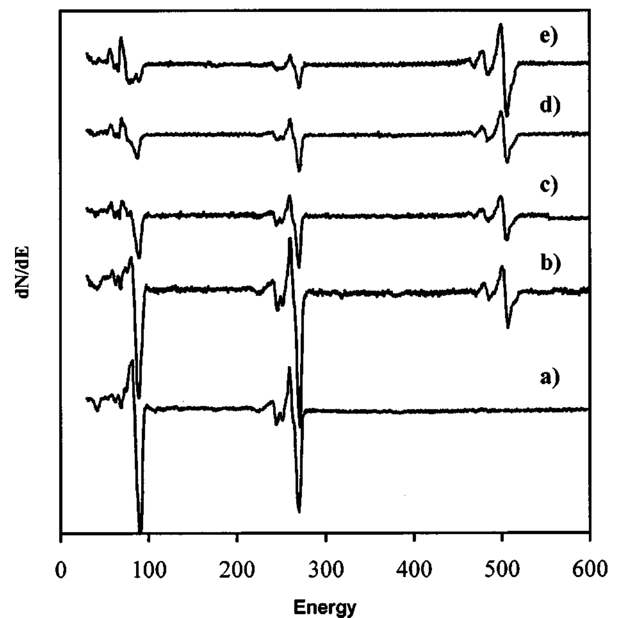

FIG. 1. AES spectra of (a) $\sqrt{3}\times\sqrt{3}$ reconstructed surface, (b) oxygen exposed SiC, (c) 30 s O-plasma exposed SiC, (d) 1 min O-plasma exposed SiC, and (e) PECVD 15 Å SiO_2 layer.

The process may be described in terms of three distinct growth stages. The initial stage is oxygen absorption onto the surface and a transition to a 1×1 reconstruction. Next, a thin oxide layer is formed on the surface. The formation of the initial oxide layer results in a surface with no LEED pattern. Finally, a thick SiO_2 layer is formed. In this study, we explore these three stages as follows: (1) a clean $\sqrt{3}\times\sqrt{3}$ surface is exposed to a low flux of O_2 at room temperature; (2) the interfacial layer is generated by two separate low temperature O_2 plasma exposures (100 °C); (3) the thick oxide is formed by plasma CVD.

For the three steps process outlined above, the AES spectra for the substrates are nearly identical after each surface preparation step. For the 4H and 6H substrates, the variance of the O, C, and Si concentrations is $<2\%$. Typical spectra for the four processes are shown in Fig. 1. From the spectra, the relative concentration of oxygen on the surface is determined by dividing the adjusted peak-to-peak height of the oxygen *KLL* by the sum of the adjusted peak-to-peak heights of the silicon *LMM*, carbon *KLL*, and oxygen *KLL* peaks. All peak-to-peak values are corrected for the Auger sensitivity factors. The relative surface concentrations of Si, O, and C are shown in Table I. For the oxygen exposed surface, the

TABLE I. Si, O, and C concentrations determined from the AES spectra.

	Si *LMM*	O *KLL*	C *KLL*
O-exposed	27%	6%	66%
30 s O-plasma	28%	11%	61%
1 min O-plasma	24%	21%	55%
PECVD SiO_2 film	28%	39%	33%

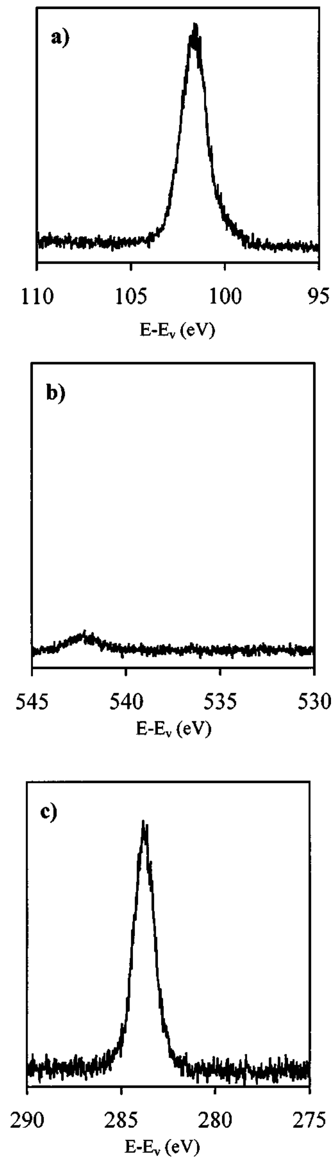

FIG. 2. XPS spectra of (a) $\sqrt{3}\times\sqrt{3}$ reconstructed surface. Core levels examined are (a) Si $2p$, (b) O $1s$, and (c) C $1s$. The spectra were excited using the Al K_α line.

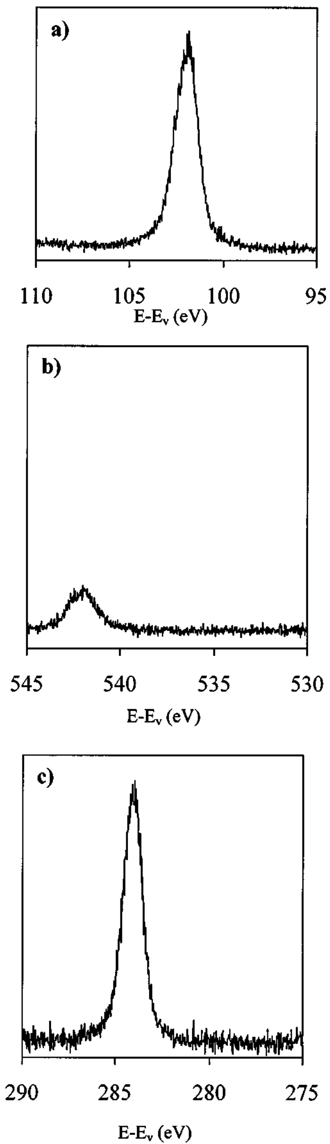

FIG. 3. XPS spectra of the oxygen exposed surface. Core levels examined are (a) Si $2p$, (b) O $1s$, and (c) C $1s$. The spectra were excited using the Al K_α line.

relative oxygen concentration is ~6% and a Si:O ratio of 4.5 is formed. The two O-plasma-treated surfaces show relative O concentrations of 11% and 21% and Si:O ratios of 2.5 and 0.9, respectively. However, the shape of the Si *LMM* peak has significantly changed between the two O-plasma treatments. The Si *LMM* peak of the first O-plasma-treated surface appears to consist of Si–O and Si–C bonding. However, the Si *LMM* peak of the second O-plasma-treated surface shows a line shape characteristic of only Si–O bonding. The PECVD deposited oxide has a relative oxygen concentration of 39% and a Si:O ratio of 0.7. Inspection of the Si *LMM* peak for the deposited oxide has the characteristic double peak indicating Si–O bonding.

For each *n*-type substrate, 4H or 6H, the XPS spectra are similar. The only differences observed in the XPS spectra are slight shifts in peak locations due to changes in the Fermi level location between substrates. For the initial $\sqrt{3}\times\sqrt{3}$ surface, there is detectable oxygen in the XPS spectra as shown in Fig. 2. The corrected oxygen concentration is ~4%. The corrected oxygen concentration is given by

$$\mathrm{Area}_{\mathrm{O}\,1s}S_{\mathrm{O}\,1s}/(\mathrm{Area}_{\mathrm{O}\,1s}S_{\mathrm{O}\,1s} + \mathrm{Area}_{\mathrm{Si}\,2p}S_{\mathrm{Si}\,2p} + \mathrm{Area}_{\mathrm{O}\,1s}S_{\mathrm{O}\,1s}),$$

where S_x is the XPS sensitivity factors for the assigned core levels, and Area_{xx} is the area of the curve fitted peak. However, examination of the Si $2p$ and C $1s$ core levels shows no detectable Si–O or C–O bonding. The location of the C $1s$ peak for the $\sqrt{3}\times\sqrt{3}$ surface is 283.8 ± 0.1 eV below the Fermi level. The XPS spectra of the oxygen exposed surface shown in Fig. 3, display a considerable increase in the oxygen concentration (13%). After a 30 s O-plasma treatment, the relative oxygen concentration via XPS is further in-

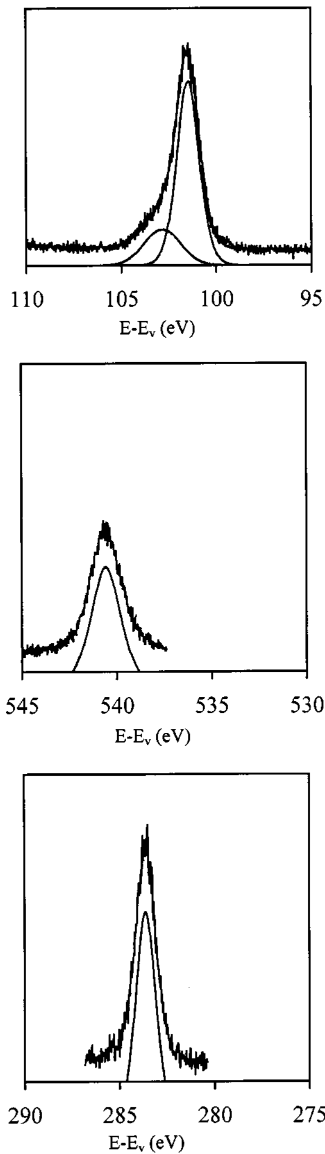

FIG. 4. XPS spectra of the 30 s O-plasma-treated surface. Core levels examined are (a) Si $2p$, (b) O $1s$, and (c) C $1s$. The spectra were excited using the Al K_α line.

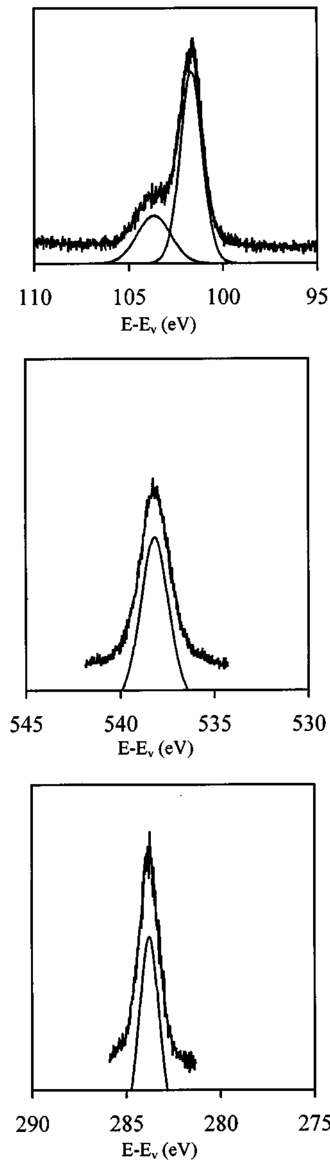

FIG. 5. XPS spectra of the 1 min O-plasma-treated surface. Core levels examined are (a) Si $2p$, (b) O $1s$, and (c) C $1s$. The spectra were excited using the Al K_α line.

creased to ~26%. There is significant Si–O bonding apparent in the XPS spectra which is shown in Fig. 4. The O $1s$ bonding energy for the O-exposed surface is 283.9 ± 0.1 eV below the Fermi level. Moreover, as shown in Fig. 5, the spectra for the 1 min O plasma, the Si–O peak intensity is again significantly increased. However, for either O plasma, there is no observable C–O bonding in the O $1s$ core level scan. For the SiO_2 deposited film, there are two definite Si peaks shown in Fig. 6. The corrected relative oxygen concentration for the SiO_2 film is 64.5%. The C $1s$ core level again reveals no significant C–O bonding. The binding energy for the C $1s$ core level that is observed after the SiO_2 layer is deposited is 283.9 ± 0.1 eV below the Fermi level.

A. *N*-type 6H SiC $(0001)_{Si}$

The UV photoemission spectra of *n*-type 6H SiC shown in Fig. 7 follow the different stages of the SiC/SiO_2 interface formation. The electronic states of the $\sqrt{3}\times\sqrt{3}$ spectra[32,33] are no longer evident in any of the various stages of the oxide growth. In particular, the in-gap surface state of the $\sqrt{3}\times\sqrt{3}$ surface is no longer evident after the initial O_2 exposure. The spectra showed no dispersion with changing of the analyzer angle. The photoemission spectra of the oxygen exposed surface of *n*-type 6H SiC show two distinct states that are indicative of oxygen. State B is located at 6.9 ±0.1 eV below the Fermi level, and state A is located at 9.5 ± 0.1 eV below the Fermi level, a difference of 2.7 ±0.1 eV.

A linear extrapolation method is used to determine the location of the VBM. The process has been outlined elsewhere. The determination of the VBM is shown in Fig. 8. The linear extrapolation of the VBM is supported by determining the VBM from the Si–C bond in the Si $2p$ core level

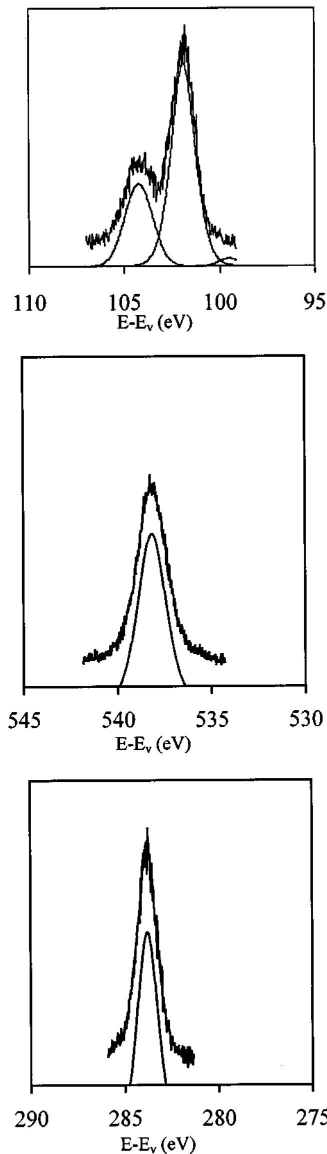

FIG. 6. XPS spectra of the PECVD SiO_2 surface. Core levels examined are (a) Si $2p$, (b) O $1s$, and (c) C $1s$. The spectra were excited using the Al K_α line.

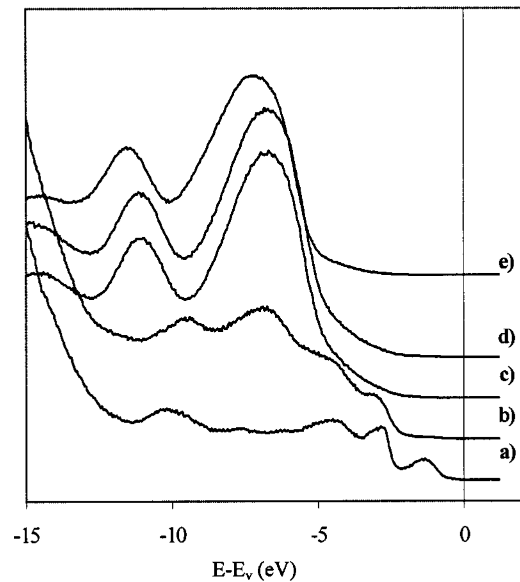

FIG. 7. UPS spectra of 6H n-type SiC (a) $\sqrt{3}\times\sqrt{3}$ reconstructed surface, (b) oxygen exposed SiC, (c) 30 s O-plasma exposed SiC, (d) 1 min O-plasma exposed SiC, and (e) PECVD 15 Å SiO_2 surfaces. Spectra were excited with He I radiation.

at 101.5 eV below the Fermi level. The energy difference of the Si–C bond from the Fermi level (101.8 eV) for the H-plasma-treated SiC surface is used to determine the SiC VBM for the various oxygen exposures.

From the width of the spectra, it is possible to determine the difference between the SiC VBM and the vacuum level. The width of the spectra is determined by measuring the energy difference between the VBM and the low-energy electron cutoff. The electron affinity χ is determined using the following relation: $\chi = h\nu - E_g - W$, where W is the width of the spectrum, E_g is the band gap, and $h\nu$ is the incident photon energy (21.2 eV). Using the equation to determine the electron affinity, the energy difference between the SiC VBM and the vacuum level ($\chi + E_g$) can easily be determined. The difference between the vacuum level and the valence band maximum (i.e., $\chi - W$) of the SiC is determined to be 7.0 ± 0.1 eV.

For the n-type 6H SiC, the locations of the peaks in the spectra are approximately equivalent for the two O-plasma exposure times. After the first 30 s exposure, state B is located at 6.7 ± 0.1 eV below the Fermi level, and state A is located at 11.0 ± 0.1 eV below the Fermi level. The energy difference between the two states is 4.3 ± 0.1 eV. Furthermore, after a second 30 s O-plasma exposure, the binding

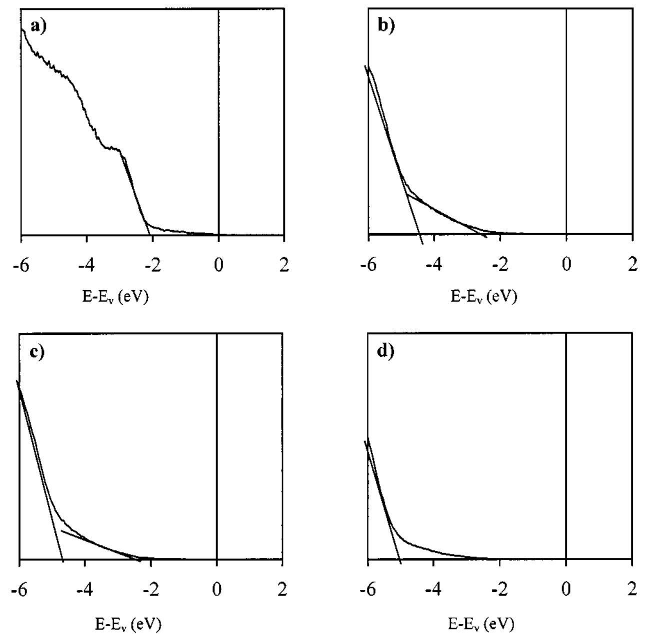

FIG. 8. VBM determination of 6H n-type SiC (a) oxygen exposed SiC, (b) 30 s O-plasma exposed SiC, (c) 1 min O-plasma exposed SiC, and (d) PECVD 15 Å SiO_2 surfaces.

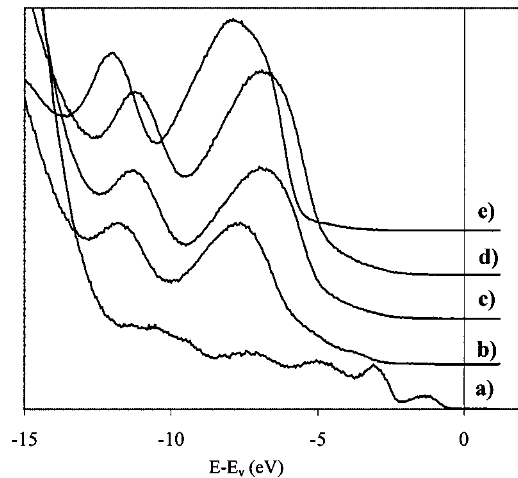

FIG. 9. UPS spectra of 4H *n*-type SiC (a) $\sqrt{3}\times\sqrt{3}$ reconstructed surface, (b) oxygen exposed SiC, (c) 30 s O-plasma exposed SiC, (d) 1 min O-plasma exposed SiC, and (e) PECVD 15 Å SiO_2 surfaces. Spectra were excited with He I radiation.

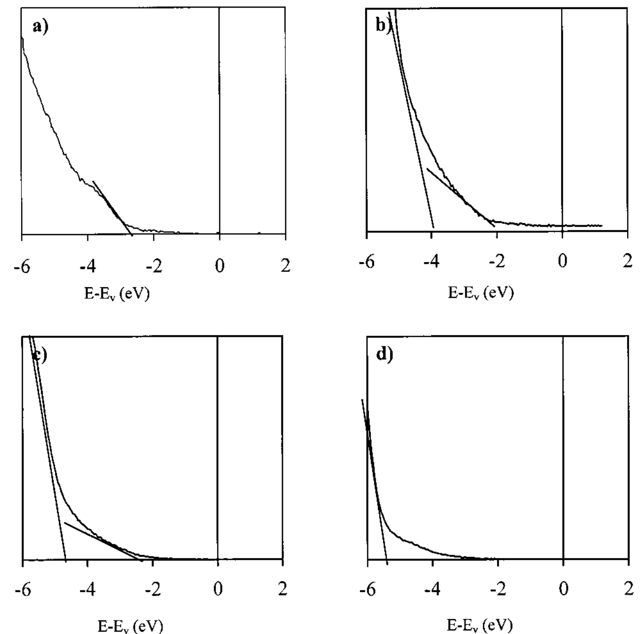

FIG. 10. VBM determination of 4H *n*-type SiC (a) oxygen exposed SiC, (b) 30 s O-plasma exposed SiC, (c) 1 min O-plasma exposed SiC, and (d) PECVD 15 Å SiO_2 surfaces.

energies of the two states are nearly unchanged. State B is located at 6.8±0.1 eV below the Fermi level, and state A is located at 11.1±0.1 eV below the Fermi level. The energy difference between the two states is also 4.3±0.1 eV.

Moreover, the O-plasma-treated surfaces exhibit a dual turn-on. The first turn-on located at 2.2±0.1 eV below the Fermi level is attributed to the SiC and the second turn-on located at 4.4±0.1 eV below the Fermi level is attributed to the oxide. The two observed VBMs directly determine the valence band offset. Furthermore, the location of the dual VBMs relative to the vacuum level is the same for the different O-plasma times. The energy difference between the SiC VBM and the vacuum level is 7.8±0.1 eV.

After oxide deposition of SiO_2 onto the *n*-type 6H SiC substrate, the photoemission properties change; the location of the oxygen bonding and antibonding states and the energy difference between the VBM and the vacuum level change. However, the energy difference between state B, located at 8.2±0.1 eV below the Fermi level, and A, located at 12.5 ±0.1 eV below the Fermi level, remained the same at 4.3 ±0.1 eV. The oxide VBM is measured to be 5.1±0.1 eV below the Fermi level. The location of the oxide VBM relative to the vacuum level is ascertained to be 10.1±0.1 eV.

B. *N*-type 4H SiC $(0001)_{Si}$

Analysis of the photoemission spectra from oxygen exposed *n*-type 4H SiC shows analogous features with the 6H SiC spectra. The photoemission spectra shown in Fig. 9 demonstrate that the locations of the features are slightly different between the two polytypes. The determination of the VBM is shown in Fig. 10. For the O-exposed surface, state B is located at 7.6±0.1 eV below the Fermi level, and state A is located 11.9±0.1 eV below the Fermi level. Again, from the width of the spectra the energy difference between the VBM and the vacuum level is determined to be 7.8 ±0.1 eV; a variance of ~1.0 eV from the 6H *n*-type SiC substrate.

The effects of the two O plasmas are similar for the *n*-type 4H SiC and the *n*-type 6H SiC. For both, the location of state B is 6.9±0.1 eV below the Fermi level, and state A is 11.2±0.1 eV below the Fermi level. The difference between the two states is 4.3±0.1 eV. The energy difference between the VBM and the vacuum level for the 4H polytype for both O-plasma exposures is 7.9±0.1 eV. The O-plasma-treated 4H SiC surfaces also exhibit a dual turn-on. The turn-on for the SiC is 2.8±0.1 eV below the Fermi level, and the turn-on for the oxide is 4.8±0.1 eV below the Fermi level.

Again, after the oxide deposition, the photoemission properties change from that of the hetero-interface to that of a SiO_2 layer. The location of the states and the energy difference between the VBM and the vacuum level change with the oxide deposition. However, the difference between state B, located at 7.7±0.1 eV below the Fermi level, and state A, located at 12.0±0.1 eV below the Fermi level, remained the same at 4.3±0.1 eV. The location of the VBM relative to the vacuum level is ascertained to be 10.0±0.1 eV. The energy difference between the VBM and the vacuum level has increased by 1.9 eV between the O-plasma processed surface and the SiO_2 layer. A summary of the values obtained from the UV photoemission spectra is shown in Table II.

IV. DISCUSSION

Investigation of the relative binding energies of states A and B can be used as an indication of the oxide formation on the surface. For the O-exposed surfaces, the relative binding

TABLE II. Values determined from the UPS spectra (in eV).

	N-type 6H SiC					
	VBM	Cutoff	S_B	S_A	ΔState (S_A-S_B)	$E_{Vac}-E_{VBM}$
O-exposure	2.2	16.7	6.8	9.5	2.7	7.0
Plasma 1	2.2	15.6	6.8	11.1	4.3	7.7
Plasma 2	2.2	15.6	6.8	11.1	4.3	7.7
SiO_2	5.1	16.1	7.2	11.5	4.3	10.1
	N-type 4H SiC					
O-exposure	2.6	16.8	7.6	11.7	4.1	6.9
Plasma 1	2.6	15.9	6.9	11.2	4.3	7.8
Plasma 2	2.6	15.9	6.9	11.2	4.3	7.8
SiO_2	5.3	16.5	7.7	12.0	4.3	9.8

energies of states A and B are 3.7 ± 0.1 and 4.1 ± 0.1 eV for 6H and 4H SiC, respectively. The lack of consistency in these values indicates that a SiO_2 film has not yet formed on the surface. However, for the O-plasma-treated surfaces and the PECVD oxide film, the relative location between states A and B is 4.3 ± 0.1 eV for both surfaces. The uniformity of the relative energies of the two states is an indication that an oxide film has formed on the surface.

The photoemission spectra (XPS and UPS) from deposited oxide film yield information of the characteristics of SiO_2 without interface effects. From the turn-on of the spectra and the energy difference between the oxide VBM and the vacuum level, it is possible to establish the band relations for the SiO_2–SiC interface. Relative to the vacuum level, the locations of several features in the photoemission spectra are identical. States A and B are at the same location from the vacuum level for each substrate. The energy for the oxygen lone pair $2p$ orbital is 12.2 ± 0.1 eV from the vacuum level, and the energy for the Si–O bond is 16.5 ± 0.1 eV from the vacuum level. These values correspond well to the accepted values of 12.15 and 16.4 eV for SiO_2 on Si.[40,41] Furthermore, the relative location of the two states to each other is 4.3 eV, which coincides with other results for the remote plasma-enhanced deposited oxide.[40]

The initial valence band offset can be directly determined from the photoemission spectra of the O-plasma exposed surfaces. The valence band offset is directly determined from the difference in the two turn-ons observed in the O-plasma processed UPS spectra. The valence band offset (ΔE_v) for the 6H SiC is determined to be 2.1 ± 0.1 eV, and ΔE_v for 4H *n*-type SiC is 2.0 ± 0.1 eV.

From the XPS spectra, a significant amount of Si–O bonding is observed which implies the formation of a film of SiO_2. It is also possible to observe both the Si–C and the Si–O bonds in the Si $2p$ core level spectrum. Using the relative location of the two core levels (2.1 eV), and the bulk values of the core levels, it is possible to determine the valence band discontinuity from the XPS spectra. The valence band discontinuity can be determined using the following equation:

$$\Delta E_v=(E^{\mathrm{I}}_{\mathrm{VBM}}-E^{\mathrm{I}}_{\mathrm{core}})-(E^{\mathrm{II}}_{\mathrm{VBM}}-E^{\mathrm{II}}_{\mathrm{core}})+(\Delta E_{\mathrm{core}}).$$

TABLE III. Values for Eq. (1) to determine the valance band discontinuity for the various substrates (in eV).

	$E^{\mathrm{I}}_{\mathrm{VBM}}$	$E^{\mathrm{I}}_{\mathrm{core}}$	$E^{\mathrm{II}}_{\mathrm{VBM}}$	$E^{\mathrm{II}}_{\mathrm{core}}$	ΔE_{core}	ΔE_v
6H *n*-type SiO	2.2	101.9	5.1	104.5	2.1	1.8
4H *n*-type SiC	2.2	101.9	5.3	104.6	2.1	1.9

The measured VBM of the clean $\sqrt{3}\times\sqrt{3}$ surface and the VBM of the SiO_2 film in conjunction with the oxide core level energies shown in Table III. The valence band discontinuities for the SiC/SiO_2 interface are $\sim2.0\pm0.1$ eV for each substrate. These values agree with the directly measured values from the UV photoemission spectra.

The band relations for the 6H SiC/SiO_2 interface and 4H SiC SiC/SiO_2 interface are shown in Fig. 11. From the plots, it is shown that the VBM for the different polytypes (6H and 4H) are at the same location relative to the oxide. This is in partial agreement with the previously reported results.[42] However, the energy difference between the VBM of the SiC and the vacuum level is ~8.0 eV compared to the previously reported 7 eV,[42] and the VB discontinuity is 2.0 eV compared to the previously reported ~3 eV. Furthermore, from the plots, the vacuum level is continuous across the interface. Using the location of the VBM relative to the vacuum level for the O-plasma-treated surfaces, and the VBM relative to the vacuum level for the SiO_2 film, the bands align following the electron affinity rule. Therefore, the electron affinity rule for VBM lineup is a valid method when using the O-plasma-treated surface and the SiO_2 film.

It should be noted that these results are significantly different from those reported by Affanas'ev.[42] Investigation of the SiO_2 photoemission spectra and the O-exposed surface photoemission spectra indicate that if the electron affinity rule is used with these surfaces, the valance band discontinuity is ~3 eV. This discrepancy should be explored further.

In order to determine band bending effects, the built-in potential (V_{Bi}) needs to be determined. Once the built-in potential is determined, the interface state density can be approximated by the relation: $n_s=\sqrt{2\kappa\epsilon_0 V_{\mathrm{Bi}}N_D/e}$, where n_s is the density of excessive charge at the surface, N_D is the doping concentration, and κ is the dielectric constant. The VBMs of the SiC for the plasma process are 2.2 ± 0.1 eV for *n*-type 6H SiC and 2.6 ± 0.1 eV for 4H SiC. These values are markedly different from the bulk values (2.94 and 3.20 eV).

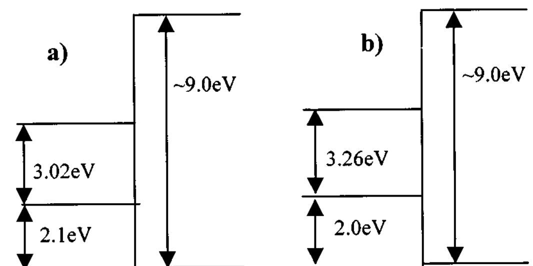

FIG. 11. Interface band relations of (a) 6H *n*-type SiC/SiO_2, and (b) 4H *n*-type SiC/SiO_2.

From the equation above, the interface state density that would cause the band bending of 0.6 eV is $\sim 5 \times 10^{12}\,cm^{-2}$.

V. CONCLUSIONS

Formation of the SiO_2/SiC heterojunction is monitored by UV photoemission. The band bending at the interface is also monitored. Plasma processing and RPECVD were used to oxidize and deposit oxides on the surface. The heterojunction band structure for the SiC/SiO_2 has been shown for 6H and 4H *n*-type SiC. The valence band offset was directly measured by ultraviolet photoemission. The valence band offsets determined by UPS are 2.1 eV for 6H *n*-type SiC and 2.0 eV for 4H *n*-type SiC. From the valence band offset and the electron affinity measurements, the use of the electron affinity rule for determining the heterojunction band offset is verified. It is evident that there is little or no change of the interface dipole at the SiC/SiO_2 interface. Furthermore, the relative location of the SiC VBM to the conduction band minimum of the SiO_2 is determined to be a constant between 6H and 4H SiC.

ACKNOWLEDGMENT

This study was supported by the Office of Naval Research.

[1]K. Hara, Mater. Sci. Forum **264–268**, 901 (1998).
[2]C. Weitzel, Mater. Sci. Forum **264–268**, 907 (1998).
[3]J. A. Powell and L. G. Matus, *Amorphous and Crystalline Silicon* (Springer, Berlin, 1989), pp. 2–12.
[4]T. P. Chow and M. Ghezzo, Mater. Res. Soc. Symp. Proc. **423**, 10 (1996).
[5]J. Cooper, M. Melloch, J. Woodall, J. Spitz, K. Schoen, and J. Henning, Mater. Sci. Forum **264–268**, 895 (1998).
[6]T. Narushima, T. Goto, Y. Yokoyama, M. Takeuchi, Y. Iguchi, and T. Hirai, J. Am. Ceram. Soc. **77**, 1079 (1994).
[7]J. B. Baliga, *Power Semiconductor Devices* (PWS, Boston, 1995).
[8]V. Khemka and T. P. Chow, J. Electrochem. Soc. **144**, 1137 (1997).
[9]B. Hornetz, H. J. Michel, and J. Halbritter, J. Mater. Res. **9**, 3088 (1994).
[10]C. Önneby and C. G. Pantano, J. Vac. Sci. Technol. A **15**, 1597 (1997).
[11]M. Maeda, K. Nakamura, T. Ohkubo, and T. Ishizuka, Ceram. Int. **15**, 1 (1989).
[12]V. M. Bermudez, J. Appl. Phys. **66**, 6084 (1989).
[13]S. Zaima, K. Onoda, Y. Koide, and Y. Yasuda, J. Appl. Phys. **68**, 6304 (1990).
[14]S. M. Tang, W. B. Berry, R. Kwor, M. V. Zeller, and L. G. Matus, J. Electrochem. Soc. **135**, C131 (1988).
[15]S. M. Tang, W. B. Berry, R. Kwor, M. V. Zeller, and L. G. Matus, J. Electrochem. Soc. **137**, 221 (1990).
[16]J. B. Casady and R. W. Johnson, Solid-State Electron. **39**, 1409 (1996).
[17]L. Muehlhoff, M. J. Bozack, W. J. Choyke, and J. T. Yates, Jr., J. Appl. Phys. **60**, 2558 (1986).
[18]S. M. Sze, *Physics of Semiconductor Devices* 2nd ed. (Wiley–Interscience, New York, 1981).
[19]S. M. Sze, *VLSI Technology*, 2nd ed. (McGraw–Hill, New York, 1988).
[20]C. S. Patuwathavithane, J. B. Crofton, J. R. Williams, C. C. Tin, Z. Feng, M. J. Bozack, P. A. Barnes, R. Ramesham, and C. D. Ellis, *Amorphous and Crystalline Silicon IV* (Springer, Berlin, 1992), pp. 163–169.
[21]J. W. Palmour, R. F. Davis, H. S. Kong, S. F. Corcoran, and D. P. Griffis, J. Electrochem. Soc. **136**, 502 (1989).
[22]L. Lipkin and J. Palmour, J. Electron. Mater. **25**, 909 (1996).
[23]A. Gölz, G. Lucovsky, K. Koh, D. Wolfe, H. Niimi, and H. Kurz, Microelectron. Eng. **36**, 73 (1997).
[24]G. Lucovsky, H. Niimi, A. Gölz, and H. Kurz, Appl. Surf. Sci. **123/124**, 435 (1998).
[25]G. Lucovsky and H. Niimi, Mater. Sci. Forum **264–268**, 1021 (1998).
[26]S. Dimitrijev, H. Li, H. Harrison, and D. Sweatman, IEEE Electron Device Lett. **18**, 175 (1997).
[27]A. Gölz, S. Scharnholz, and H. Kurz, Microelectron. Eng. **36**, 187 (1997).
[28]H. Li, S. Dimitrijev, H. Harrison, and D. Sweatman, Appl. Phys. Lett. **70**, 2028 (1997).
[29]S. Sridevan, V. Misra, P. K. McLarty, B. J. Baliga, and J. J. Wortman, IEEE Electron Device Lett. **16**, 524 (1995).
[30]U. Starke, M. Kranke, J. Bernhardt, J. Schardt, K. Reuter, and K. Heinz, Mater. Sci. Forum **264–268**, 321 (1998).
[31]L. Johansson, F. Owman, P. Martensson, C. Persson, and U. Lindefelt, Phys. Rev. B **53**, 13803 (1996).
[32]L. Johannson, F. Owman, and P. Martensson, Surf. Sci. **360**, L483 (1996).
[33]T. Jikimoto, T. Tsukamoto, A. Kinoshita, Y. Satoh, M. Hirai, M. Kusaka, M. Iwami, and T. Nakata, Appl. Surf. Sci. **117/118**, 794 (1997).
[34]T. Tsukamoto, M. Hirai, M. Kusaka, M. Iwami, T. Ozawa, T. Nagamura, and T. Nakata, Appl. Surf. Sci. **113/114**, 467 (1997).
[35]L. Johannson, F. Owman, and P. Martensson, Phys. Rev. B **53**, 13793 (1996).
[36]M. Sabisch, P. Krüger, and J. Pollmann, Phys. Rev. B **55**, 10561 (1997).
[37]I. Forbeaux, J. M. Themlin, V. Langlais, L. Yu, H. Belkhir, and J. M. Debever, Surf. Rev. Lett. **5**, 193 (1998).
[38]L. Johansson, F. Owman, and P. Martensson, Surf. Sci. **360**, L478 (1996).
[39]J. van der Weide and R. J. Nemanich, J. Vac. Sci. Technol. B **10**, 1940 (1992).
[40]K. Hirose, H. Nohira, T. Koike, T. Aizaki, and T. Hattori, Appl. Surf. Sci. **123/124**, 542 (1998).
[41]H. Nohira, A. Omura, M. Katayama, and T. Hattori, Appl. Surf. Sci. **123/124**, 546 (1998).
[42]V. V. Afanas'ev, M. Bassler, G. Pensl, and M. J. Schulz, J. Appl. Phys. **79**, 3108 (1996).